

1 **Supplemental Material**

2 **Bacterial strains and oligonucleotides used in this work**

3 See Tables S1A and S1B below. Growth curves in Fig. S8.

4 **Analysis of diffusive behavior**

5 *Mean-square displacement plots $MSD(\tau)$*

6 The MSD as a function of lag time τ is given by $MSD(\tau) = \langle (\mathbf{r}(t + \tau) - \mathbf{r}(t))^2 \rangle$, where
7 $\mathbf{r}(t)$ is the two-dimensional location of the particle at time t , τ is the lag time, and the average is
8 taken over all times t and over many trajectories. $MSD(\tau)$ plots for the different species and
9 imaging conditions are shown in Fig. 2. The slope of the first two points of an $MSD(\tau)$ plot
10 provides a first estimate of the mean diffusion coefficient: $D = \text{slope}/4$. The MSD slope takes
11 account of the localization error σ (1), but does not account for confinement effects. Even for
12 $6 \times 2 \text{ ms} = 12 \text{ ms}$ long trajectories, for rapidly diffusing species with $D \sim 5 \mu\text{m}^2\text{-s}^{-1}$ confinement
13 restricts diffusive trajectories and causes curvature of the MSD plot. This makes the diffusion
14 coefficient from the two-point slope a lower bound on the true mean D . The trajectory analysis
15 presented below is more accurate.

16 *Estimation of dynamic localization error σ_{fast} and σ_{slow} for fast and slow EF-Tu molecules*

17 Localization error in the single-step $P(r)$ distributions arises from the point-spread function
18 (PSF) of the microscope, the finite number of photons detected per camera frame, and blurring of
19 the images due to diffusive motion during each 2 ms camera frame (1, 2). While ribosomes and
20 slow EF-Tu copies experience little diffusive blurring, the fast EF-Tu copies are blurred
21 substantially. We reasoned that model Monte Carlo diffusive trajectories should involve larger
22 dynamic localization error for fast EF-Tu copies than for slow EF-Tu copies.

23 This problem has been addressed in detail by Michalet (1). Suppose the best fit to the first
 24 two experimental points of a two dimensional mean-square displacement plot is given by the
 25 equation $MSD(\tau) = a + b\tau$, with b the slope and a the extrapolated intercept at lag time $\tau = 0$.
 26 Then the best estimate of the diffusion coefficient is $D = b/4$ and the best estimate of the dynamic
 27 localization error is $\sigma = \frac{1}{2} (a + 4Dt_E/3)^{1/2}$, where t_E is the exposure time per camera frame. We
 28 estimate that the diffusion coefficient of the fast (non-ribosome-bound) EF-Tu copies should be
 29 about $5 \mu\text{m}^2\text{-s}^{-1}$ (3, 4) and that of the ribosome-bound copies should be about $0.2 \mu\text{m}^2\text{-s}^{-1}$ (5). If
 30 so, the root-mean-square displacement in two dimensions of a fast EF-Tu copy during the 2-ms
 31 camera frame is ~ 200 nm, substantially larger than typical static localization errors in live *E. coli*
 32 single-molecule studies of slowly moving species labeled with fluorescent proteins. The rms
 33 displacement of a ribosome-bound EF-Tu copy is only ~ 60 nm, comparable to typical static
 34 localization errors.

35 For WT EF-Tu, the intercept of the MSD plot yields a mean localization error $\sigma = 60$ nm.
 36 To estimate the dynamic localization errors σ_{fast} and σ_{slow} for EF-Tu, we simulated six-step
 37 (6 x 2 ms) Monte Carlo diffusive trajectories in a model spherocylinder. One batch of 5000
 38 trajectories had $D_{slow} = 0.2 \mu\text{m}^2/\text{s}$ and the other 5000 trajectories had $D_{fast} = 5 \mu\text{m}^2/\text{s}$; both used
 39 the mean localization error of 60 nm. These simulated trajectories were used to form the
 40 distribution of the mean of six one-step estimates of D :

41 $\langle D \rangle_{6\text{-step}} = \frac{1}{24\tau} \sum_{i=1}^6 \sqrt{(x_{i+1} - x_i)^2 + (y_{i+1} - y_i)^2}$, where (x_{i+1}, y_{i+1}) and (x_i, y_i) are the

42 coordinates of final and initial positions of each step. This distribution is shown in Fig. S6A.

43 For WT EF-Tu, the analogous experimental distribution of $\langle D \rangle_{6\text{-step}}$ is shown in Fig. S6B. The
 44 simulated distributions guided the choice of cutoffs that approximately distinguish slow from fast
 45 copies: $< 2.25 \mu\text{m}^2/\text{s}$ for slow copies and $> 3.25 \mu\text{m}^2/\text{s}$ for fast copies. Separate MSD plots for

46 these slow and fast experimental trajectories are shown in Fig. S6C. The intercepts of the linear
47 fits to the first two data points gives the estimates $\sigma_{\text{slow}} \sim 40$ nm and $\sigma_{\text{fast}} \sim 80$ nm. These values
48 were used to simulate trajectories for fitting the $P_{EF-Tu}(r)$ distributions to two static populations.

49 **Monte Carlo simulations of diffusive trajectories**

50 Many previous studies of single-molecule diffusion fit the experimental $P(r)$ distribution to
51 a sum of analytical functions, with each component describing diffusion of the species in free
52 space (6, 7). However, molecules diffusing rapidly in the *E. coli* cytoplasm suffer from
53 confinement due to the spherocylindrical cell boundaries, a problem for which there is no
54 analytical solution. Therefore, we simulated the behavior of each diffusive component from a
55 large number of random walk trajectories that incorporate the dynamic localization error σ_{slow} or
56 σ_{fast} and confinement effects within a model spherocylinder that mimics the dimensions of a
57 typical *E. coli* cell in our growth conditions (tip-to-tip cell length = 4.3 μm and
58 cell diameter = 0.9 μm). Each set of simulations models one diffusive state, with values of D and
59 σ fixed. At $t = 0$, 5000 particles were randomly distributed within the cell volume. Each particle
60 undergoes a random walk independent of other particle positions. To model each 2-ms camera
61 image, three-dimensional microtrajectories (1000 steps of 2 μs each) were generated. At each
62 time step, each particle chooses a displacement in each of three Cartesian directions. These
63 displacements are chosen from a Gaussian distribution whose standard deviation corresponds to
64 the state's three-dimensional diffusion coefficient D . In the rare event that a particle attempts to
65 step outside of the cell boundaries, the displacement for that microstep is taken to be zero. The
66 location of each particle during each camera frame is obtained as the centroid of the model
67 microtrajectories in order to mimic the analysis procedure used for the experimental images. The
68 appropriate dynamic localization error σ was then applied to each centroid location in both x and
69 y coordinates by sampling a Gaussian distribution with standard deviation σ . By adding the error

70 to the centroid position we obtain the model “measured” location for each 2 ms camera frame.
 71 The x and y coordinates of each measured location are stored for further analysis. For the next
 72 model camera frame, each particle continues to make microsteps in 3D starting from the
 73 endpoint of the previous camera frame. Model trajectories for EF-Tu use the appropriate
 74 estimated value of σ_{slow} or σ_{fast} , determined as described above.

75 By connecting the sequence of simulation locations over seven frames, we form 5000 model
 76 trajectories for each relevant value of D . These trajectories are used to compute model-based,
 77 numerical one-step probability distributions $P_{\text{model}}(r;D)$ that are the model functions for the
 78 least-squares analysis of the corresponding experimental distributions.

79 *Fitting of single-step $P(r)$ distributions to static, two-state models*

80 For each species in each experimental condition, a large set of trajectories that lasted for
 81 6 steps or longer were selected for analysis. Longer trajectories were truncated to 6 steps.

82 The 6-step trajectories were then sliced into individual steps. The single-step displacements

83 $r_i = \sqrt{(x_{i+1} - x_i)^2 + (y_{i+1} - y_i)^2}$ were pooled to form the distribution $P(r)$, as in Figs. 3A and

84 4C. We typically attempt to fit the experimental distribution $P(r)$ in a least-squares sense to a

85 single population or to a weighted average of two static populations. For a one-state model the

86 only fitting parameter is D . For unconstrained models including two static (non-exchanging)

87 states, the fitting function is the linear combination $P_{\text{model}}(r) = f_{\text{slow}}P(r;D_{\text{slow}}) + (1 - f_{\text{slow}})P(r;D_{\text{fast}})$.

88 Here the three fitting parameters are D_{fast} , D_{slow} , and the fractional population f_{slow} , which in turn

89 fixes $f_{\text{fast}} = (1 - f_{\text{slow}})$. For all our fitting procedures, D_{fast} ranged from 0.1 to 12 $\mu\text{m}^2/\text{s}$ with

90 interval of 0.1 $\mu\text{m}^2/\text{s}$ and D_{slow} ranged from 0.05 to 3 $\mu\text{m}^2/\text{s}$ with interval of 0.05 $\mu\text{m}^2/\text{s}$.

91 We judge the goodness of fit by evaluating the reduced chi-square statistic:

92
$$\chi_v^2 = \frac{1}{(N - \alpha)} \sum_{j=1}^N \frac{(h_j - y_j)^2}{s_j^2}$$
. Here j labels the N bins in the (unnormalized) $P(r)$ and $P_{\text{model}}(r)$

93 histograms, h_j is the number of experimental counts in bin j , y_j is the number of counts in bin j of
94 the simulated $P_{model}(D_i)$ histogram, s_j^2 is the variance of the value in bin j , and α is the number of
95 fitted parameters. We take $s_j^2 = h_j$ as the estimate of the variance, assuming Poisson statistics.

96 A good fit to an adequately flexible *analytical* model function should have $\chi_v^2 \sim 1$. In our
97 numerical procedure, both the experimental distribution $P(r)$ and the fitting function $P_{model}(r)$
98 have noise, so we would expect good fits to have χ_v^2 values somewhat larger than 1. The fitting
99 results for each species in various conditions are summarized in the main text and in Table 1.

100 To estimate the uncertainty in the model parameters for two-state fits, we examined the 3D
101 grid of χ_v^2 values generated from the unconstrained fits that varied all three parameters D_{fast} , f_{slow} ,
102 and D_{slow} . For WT EF-Tu, three two-dimensional planes passing through the values
103 $D_{fast} = 4.9 \mu\text{m}^2\text{-s}^{-1}$, $f_{slow} = 0.60$, and $D_{slow} = 1.0 \mu\text{m}^2\text{-s}^{-1}$ are shown in Fig. S7. We judged the fits
104 to be qualitatively poor whenever the value of χ_v^2 exceeded the minimum value by 0.5 units or
105 more (Fig. S7). The parameter error estimates in Table 1 cover this range of χ_v^2 values in each
106 case.

107 ***Fitting of single-step $P_{EF-Tu}(r)$ distributions to static, three-state models***

108 We briefly explored three-state models (slow, fast, and medium) of the WT EF-Tu $P(r)$
109 distribution of Fig. 3A. To make the search tractable, the slow and fast diffusion coefficients
110 were fixed to 0.1 and 4.9 $\mu\text{m}^2/\text{s}$, mimicking ribosome-bound and free EF-Tu states. The slow and
111 the medium fractions were varied in intervals of 0.05 and the medium fraction diffusion
112 coefficient D_{medium} from 0.1-5 $\mu\text{m}^2/\text{s}$ in intervals of 0.1 $\mu\text{m}^2/\text{s}$. The fast fraction was determined
113 as $f_{fast} = 1 - f_{slow} - f_{medium}$. The best fit parameters were $f_{slow} = 0.20 \pm 0.05$, $f_{medium} = 0.45 \pm 0.05$,
114 and $D_{medium} = 1.8 \pm 0.5 \mu\text{m}^2/\text{s}$, with $f_{fast} = 0.35 \pm 0.05$ and $\chi_v^2 = 1.25$ (Fig. S1C). This is no better
115 fit than the best two-state model, which returned $\chi_v^2 = 1.24$. For the three-state fit, $f_{slow} + f_{medium} =$

116 0.65 is in sensible agreement with the two-state result $f_{slow} = 0.60$. These fits are not very
117 different in content. The sum of the slow and medium components in the best three-state fit is
118 quite similar to the slow component of the best two-state fit.

119 **Statistics of aa-tRNA sampling**

120 The time-averaged stoichiometry of EF-Tu and tRNA binding to a translating 70S ribosome
121 can be estimated from the fraction of EF-Tu copies bound to ribosomes combined with copy
122 number estimates from other studies. There are 61 different codons and 43 different aa-tRNA
123 types (43 different ternary complexes) used by *E. coli* (8). Forty-eight codons match only one
124 type of ternary complex, 12 match two types, and one matches three types. This means that the
125 ribosome is usually testing and rejecting non-cognate or near-cognate aa-tRNAs. In turn, this
126 means the A site is most frequently occupied by an aa-tRNA within its ternary complex, still
127 tethered to L7/L12 (prior to GTP hydrolysis and ejection of EF-Tu).

128 Fully 40 unique codons are used with at least 1% frequency (9). For a given mRNA codon
129 poised at the 30S decoding site, the average chance that a particular ternary complex carries a
130 cognate (completely matching) aa-tRNA anticodon is roughly 1 in 40. How many different
131 ternary complexes must be sampled before a cognate aa-tRNA is found? For simplicity, we
132 assume that there are N different aa-tRNA types (N different anti-codons) all required with equal
133 probability in the transcriptome and all equally represented in the pool of aa-tRNA. This enables
134 calculation of a closed form for the mean number of trials required to find an anti-codon that
135 matches the current mRNA codon at the ribosome A site. Let $p = 1/N$ be the probability of a
136 match on a given trial. The index k denotes the number of individual trials required to achieve a
137 codon match. If the sampling of the pool is random, then the probability $P(k)$ of finding the first
138 match on the k th trial is the probability of failing to find a match for $(k - 1)$ successive trials,

139 which is $(1 - p)^{k-1}$, times the probability of finding a match on the k th trial: $P(k) = (1 - p)^{k-1} p$.

140 The average number of trials required to find a match is:

$$\begin{aligned} 141 \quad \langle k \rangle &= \sum_{k=1}^{\infty} k P(k) = \sum_{k=1}^{\infty} k (1 - p)^{k-1} p \\ 142 \quad &= p \sum_{k=1}^{\infty} k (1 - p)^{k-1}. \end{aligned}$$

143 Let $x = (1 - p)$. Then:

$$\begin{aligned} 144 \quad \langle k \rangle &= (1 - x) \sum_{k=1}^{\infty} k x^{k-1} \\ 145 \quad &= (1 - x) \frac{d}{dx} \sum_{k=1}^{\infty} x^k \quad \text{This is the derivative of a geometric series, which can be summed:} \\ 146 \quad &= (1 - x) \frac{d}{dx} \frac{x}{1 - x} = \frac{1}{1 - x} = \frac{1}{p}. \end{aligned}$$

147 For $p = 1/N$, the mean number of trials required to find a match is N . If $N \sim 40$, on average
148 roughly 40 ternary complexes must be sampled before finding a cognate codon.

149 **Estimates of copy numbers and partitioning of EF-Tu and tRNA**

150 Under the same growth conditions used here (30°C in EZRDM), we previously estimated
151 ~50,000 30S ribosomal subunits per cell, some 80% of which (~40,000 copies) are engaged as
152 translating, 70S ribosomes (10). Mean copy number estimates for EF-Tu, total tRNA, EF-G, and
153 total aa-tRNA synthetase (Table S1C) were derived from the ribosome copy number and from
154 literature values of the ratio of each species' copy number to that of ribosomes. It was not
155 possible to match strains, growth conditions, growth rate, and temperature, so we chose to match
156 the growth rate (~1 doubling/hr).

157 EF-Tu is the most abundant protein in *E. coli*, about 7-fold more abundant than ribosomes
158 (11, 12) (~350,000 total EF-Tu copies). The two-state analysis of $P_{EF-Tu}(r)$ in Fig. 3A combined
159 with the axial distribution of these slowly diffusing copies indicates that ~60% of EF-Tu copies
160 (~210,000) locate in the 70S-rich regions of space, where they undergo rapid exchange between

161 the ribosome-bound state (80% of the time) and rapidly diffusing state (20% of the time) on a
162 timescale of ~2 ms or less. At a given moment, this corresponds to ~170,000 ribosome-bound
163 EF-Tu copies ($0.8 \times 0.6 \times 350,000$). The remaining ~180,000 EF-Tu copies comprise free ternary
164 complexes and bare EF-Tu seeking an aa-tRNA partner. The ~170,000 ribosome-bound EF-Tu
165 copies is four times the estimated number of translating, 70S ribosomes. In *E. coli*, there are four
166 L7/L12 sites per 50S subunit (13, 14). Under the assumption that ternary complexes bind to the
167 ribosome only when interacting with L7/L12 N-terminal domains (further justified below), we
168 infer that the four L7/L12 sites are essentially saturated with EF-Tu copies. An equilibrium
169 binding calculation (below) corroborates this conclusion.

170 This analysis ignores the fact that each time a cognate aa-tRNA binds to the A site and
171 transfers its aminoacyl group to the growing peptide chain, elongation factor G (EF-G) must bind
172 to the A site and hydrolyze GTP in order to drive translocation of the A site tRNA to the P site
173 and the P site tRNA to the E site. EF-G uses the same ribosomal L7/L12 sites as EF-Tu for its
174 initial binding step (15). A tethered EF-G presumably samples the A site in much the same way
175 as a tethered ternary complex. The estimated copy number of EF-G is 6-7 times smaller than that
176 EF-Tu (11), *i.e.*, the EF-G copy number is similar to that of the ribosomes. *In vitro* studies found
177 that EF-Tu and EF-G have comparable binding constants to L7/L12 units (16). Accordingly, we
178 suggest that the mean occupancy of the four L7/L12 sites is ~3.5 EF-Tu copies ($7/8 \times 4$) and ~0.5
179 EF-G copies ($1/8 \times 4$). This seems a reasonable fractional occupancy of EF-G to ensure that a
180 cognate aa-tRNA at the A site need not wait long for the arrival of an EF-G(GTP) copy to drive
181 translocation. There is only one type of EF-G vs 43 types of ternary complex, so each EF-G visit
182 to an L7/L12 site will be much more effective than each ternary complex visit.

183 So far, we have estimated that averaged over time, each ribosome binds ~3.5 ternary
184 complexes (3.5 EF-Tu and 3.5 tRNA) and 0.5 EF-G copies, all tethered to L7/L12 subunits. One

185 of the ternary complexes typically occupies the A site. Next we estimate the partitioning of total
186 tRNA among different species. The total tRNA copy number in *E. coli* growing at 1–2
187 doublings/hr is ~7-fold larger than the ribosome copy number (17). This implies $\sim 7 \times 50,000 =$
188 350,000 total tRNA per cell in our growth conditions, the same as the estimated EF-Tu copy
189 number. We estimate that averaged over time, each translating ribosome binds one tRNA in the
190 A site (usually tethered to an L7/L12 via an EF-Tu bridge), one in the P site, perhaps one-half
191 copy in the E site (a compromise between “2-1-2” and “2-3-2” elongation models (18, 19)), and
192 an additional 2.5 copies bound as ternary complexes to the other three L7/L12 sites. Thus the
193 time-averaged number of tRNA copies bound to each translating ribosomes is about 5. The
194 ~40,000 translating ribosomes per cell in our growth conditions would then bind ~200,000 tRNA
195 copies at a given moment in time (~57% of all copies). On average, 3.5 of these 5 copies
196 (140,000) are associated with EF-Tu as ternary complexes and the other 1.5 copies (60,000) are
197 ribosome-bound at the P and E sites and not associated with EF-Tu. The remaining ~150,000
198 tRNA copies (~43%) are not ribosome-bound and should partition among three diffusive states:
199 free tRNA shortly after leaving the ribosomal E site, tRNA being recharged by aa-tRNA
200 synthetase, and tRNA within ternary complexes.

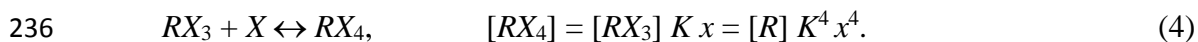
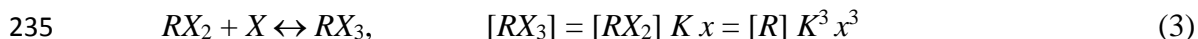
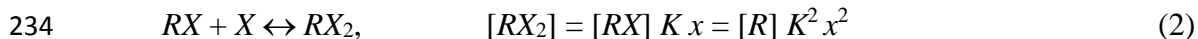
201 A simple equilibrium calculation indicates that a large majority of the 290,000 tRNA copies
202 not engaged at the ribosomal P and E sites should form ternary complexes and that most of the
203 350,000 EF-Tu copies also occur as ternary complexes. The binding constant *in vitro* between
204 tRNA and EF-Tu has been measured to be $K_b = 7.5 \mu\text{M}^{-1}$ (20). Binding constants are expected to
205 be larger in the crowded cytoplasm than in buffer solution (21). The volume of an average,
206 ~4 μm long, 0.9 μm diameter spherocylindrical cell is $V_{cell} = 2.35 \mu\text{m}^3$. For that volume, each
207 1000 copies corresponds to a concentration of 0.71 μM . As an illustrative calculation, suppose
208 we mixed 350,000 free EF-Tu copies (248 μM) with 290,000 free tRNA copies (206 μM) in the

209 cytoplasm. The solution-phase binding constant then predicts that at equilibrium, there will be
210 289,000 ternary complexes (accounting for 82% of all EF-Tu), 60,000 free EF-Tu copies, and
211 only 1,000 free tRNA copies. However, that calculation neglects the tRNA copies that are bound
212 to the 20 types of aa-tRNA synthetase, whose aggregate copy number is ~50,000 (11). In the
213 limit of saturation of the synthetases with tRNA, only 240,000 tRNA copies would be available
214 for binding with EF-Tu to form ternary complexes. At equilibrium, a mixture of 350,000 EF-Tu
215 with 240,000 tRNA would yield 240,000 ternary complexes and 110,000 free EF-Tu. Roughly
216 70% of the EF-Tu would still exist as ternary complexes. The tRNA copies would then occur as
217 240,000 ternary complexes, 60,000 P- and E-site copies, 50,000 complexes with the synthetase,
218 and only 400 free tRNA copies. This is the estimate used in the main text. Free tRNA is a small
219 minority population in either equilibrium estimate.

220 Assuming the smaller estimate of 240,000 ternary complexes, we can use a second binding
221 equilibrium calculation to estimate the average number of ternary complexes bound to the four
222 L7/L12 units on each translating ribosome. *In vitro*, the binding constant between a single
223 L7/L12 unit and a ternary complex is $K_b = 0.1 \mu\text{M}^{-1}$ (16). Again, this likely underestimates the
224 binding constant *in vivo*. Assume the cytoplasm initially contained 240,000 ternary complexes
225 (170 μM) and 40,000 translating ribosomes (28 μM). Further assume independent binding
226 (no cooperativity) of four ternary complexes to the four L7/L12 units on each 70S ribosome (22).
227 Then at equilibrium the average number of ternary complexes bound to each 70S ribosome is
228 3.8 out of a maximum of 4.

229 The binding model goes as follows. Let R stand for a 70S ribosome and X stand for a ternary
230 complex. Equilibrium concentrations are denoted by square brackets; for simplicity, $x = [X]$.

231 There are four sequential binding equilibria, each with the same binding constant K and its own
232 equilibrium equation:



237 Let R_0 be the total ribosome concentration and X_0 be the total ternary complex concentration:

238 $R_0 = [R] + [RX] + [RX_2] + [RX_3] + [RX_4] \quad (5)$

239 $X_0 = x + [RX] + 2[RX_2] + 3[RX_3] + 4[RX_4] \quad (6)$

240 Substituting Eqs. 1-4 into equations 5 and 6 and solving for $[R]$ and for $(X_0 - x)$ yields two
241 expressions for $[R]$:

242 $[R] = R_0 / (1 + Kx + K^2x^2 + K^3x^3 + K^4x^4) \quad \text{and} \quad (7)$

243 $[R] = (X_0 - x) / (Kx + 2K^2x^2 + 3K^3x^3 + 4K^4x^4) \quad (8)$

244 For given values of K and the initial concentrations R_0 and X_0 , equations 7 and 8 can be set equal
245 to each other and solved for x , whose value then determines all the equilibrium concentrations. In
246 practice, we solved the equation by trial and error using an Excel spreadsheet.

247 These rough estimates based on solution-phase binding constants may well underestimate
248 the extent of complex formation, both for formation of ternary complexes from EF-Tu and aa-
249 tRNA and for binding of ternary complexes to L7/L12 units. The estimates help to justify the
250 assertion that at a given moment most EF-Tu copies exist as ternary complexes. They are also
251 consistent with the assertion that the four L7/L12 sites on each 70S ribosome are essentially
252 saturated with ~ 4 bound ternary complexes. Finally, they predict that only a very small fraction
253 of tRNA, perhaps 1% or less, exists as the free, unbound species.

254

255 ***In vivo* rate constants for binding and unbinding of ternary complexes**

256 Finally, we can estimate two *in vivo* rate constants for direct comparison with the recent set
257 of theoretical *in vivo* rate constants derived from a large set of *in vitro* measurements obtained
258 under standardized experimental buffer conditions and temperature. Our interpretation of the
259 value $D_{slow} = 1.0 \mu\text{m}^2\text{-s}^{-1}$, as a composite of 80% ribosome-bound copies and 20% free copies,
260 suggests that the timescale for bound-free exchange *within the ribosome-rich regions* must be 2
261 ms or less. This constrains the ratio $\tau_{on}/\tau_{off} = 4$ and the sum $(\tau_{on} + \tau_{off}) \leq 2$ ms. For concreteness,
262 assume that $(\tau_{on} + \tau_{off}) = 2$ ms, which yields the values $\tau_{off} = 0.4$ ms and $\tau_{on} = 1.6$ ms. The time
263 τ_{off} is the mean search time for a ternary complex to find an empty L7/L12 site within the
264 ribosome-rich regions.

265 First we use the pseudo-first-order rate τ_{off}^{-1} and the 70S ribosome concentration to estimate
266 the effective bimolecular association rate constant k_1 for binding of a typical non-cognate ternary
267 complex to an L7/L12 subunit of a 70S ribosome within the ribosome-rich regions. Suppose the
268 40,000 70S ribosomes occupy roughly half of the $2.4 \mu\text{m}^3$ volume of the average cell; then the
269 concentration of translating ribosomes within the ribosome-rich regions is $[70S] \sim 55 \mu\text{M}$. The
270 effective bimolecular rate constant becomes $k_1 = \tau_{off}^{-1}/[70S] = 4.5 \times 10^7 \text{ M}^{-1}\text{s}^{-1}$. This is
271 remarkably fast, and if $(\tau_{on} + \tau_{off})$ were < 2 ms, the estimate would be even larger. For
272 comparison, the diffusion-limited bimolecular rate constant for ribosomal spheres of radius R_{ribo}
273 $= 10$ nm and diffusion coefficient $D_{ribo} = 0.1 \mu\text{m}^2/\text{s}$ colliding with ternary complex spheres with
274 $R_{TC} = 2$ nm and $D_{TC} = 5 \mu\text{m}^2/\text{s}$ is $k_{diff} = 4\pi N_0(R_{ribo} + R_{TC})(D_{ribo} + D_{TC}) = 3.2 \times 10^8 \text{ M}^{-1}\text{s}^{-1}$, only
275 sixfold larger than our estimated k_1 . Roughly one in six close encounters between a ternary
276 complex and a 70S ribosome, leads to a binding event. As suggested earlier (13), k_1 may be very
277 fast due to the presence of four L7/L12 binding sites per ribosome and the flexibility of the

278 linkages between ribosome and the C-terminal domain of L7/L12. We call k_1 an effective rate
279 constant because in many close encounters the ternary complex will find most L7/L12 binding
280 sites already occupied by a ternary complex or an EF-G, unlike pseudo-first-order conditions
281 used in kinetics assays. The theoretical *in vivo* estimate for κ_{on}^* (Table 2 of Ref. (8)) at 1.07
282 doublings/hr and 37°C is $9.4 \times 10^7 \text{ M}^{-1}\text{s}^{-1}$, twofold larger than our lower limit on k_1 .

283 We can also compute the unimolecular dissociation rate of EF-Tu (typically part of a ternary
284 complex) from the ribosome, $k_{-1} = \tau_{on}^{-1} \geq 625 \text{ s}^{-1}$ at 30°C with the theoretical *in vivo* rate for 1.07
285 doublings/hr at 37°C. The latter is $\omega_{off}^* = 1700 \text{ s}^{-1}$ (Table 2 of Ref. (8)). Correcting from our
286 30°C to 37°C increases k_{-1} by a factor of 2.1: $k_{-1}(37^\circ\text{C}) = 2.1 k_{-1}(30^\circ\text{C}) \geq 1250 \text{ s}^{-1}$. The effects of
287 temperature on k_{-1} were derived from the T -dependence of the experimental *in vitro* rate
288 constants in Table 1 of Ref. (8): $k_{-1} = 85 \text{ s}^{-1}$ at 20°C and 700 s^{-1} at 37°C. We assumed the
289 Arrhenius temperature dependence with A-factor independent of T : $k_{-1}(T) = A \exp[-E_a/RT]$, with
290 E_a the activation energy and R the gas constant.

291

378 **Supplemental References**

- 379 1. Michalet X. 2010. Mean Square Displacement Analysis of Single-Particle Trajectories
380 with Localization Error: Brownian Motion in Isotropic Medium. *Phys Rev E Stat Nonlin*
381 *Soft Matter Phys* 82:041914-041914.
382
- 383 2. Thompson RE, Larson DR, Webb WW. 2002. Precise nanometer localization analysis for
384 individual fluorescent probes. *Biophys J* 82:2775-2783.
385
- 386 3. Nenninger A, Mastroianni G, Mullineaux CW. 2010. Size dependence of protein
387 diffusion in the cytoplasm of *Escherichia coli*. *J Bacteriol* 192:4535-40.
388
- 389 4. Bakshi S, Bratton BP, Weisshaar JC. 2011. Subdiffraction-limit study of Kaede diffusion
390 and spatial distribution in live *Escherichia coli*. *Biophys J* 101:2535-44.
391
- 392 5. Mohapatra S, Choi H, Ge X, Sanyal S, Weisshaar JC. 11 May 2017. Spatial Distribution
393 and Ribosome-binding Dynamics of EF-P in Live *E. coli*. *mBio*
394 doi:10.1128/mBio.00300-17.
395
- 396 6. Chen T-Y, Santiago AG, Jung W, Krzemiński Ł, Yang F, Martell DJ, Helmann JD, Chen
397 P. 2015. Concentration- and chromosome-organization-dependent regulator unbinding
398 from DNA for transcription regulation in living cells. *Nat Commun* 6:7445.
399
- 400 7. Plochowitz A, Farrell I, Smilansky Z, Cooperman BS, Kapanidis AN. 2017. In vivo
401 single-RNA tracking shows that most tRNA diffuses freely in live bacteria. *Nucleic*
402 *Acids Res* 45:926-937.
403
- 404 8. Rudolf S, Thommen M, Rodnina MV, Lipowsky R. 2014. Deducing the kinetics of
405 protein synthesis in vivo from the transition rates measured in vitro. *PLoS Comput Biol*
406 10:e1003909.
407
- 408 9. Maloy S, V. Stewart, and R. Taylor. 1996. Genetic analysis of pathogenic bacteria. Cold
409 Spring Harbor Laboratory Press, NY.
410
- 411 10. Bakshi S, Choi H, Weisshaar JC. 2015. The spatial biology of transcription and
412 translation in rapidly growing *Escherichia coli*. *Front Microbiol* 6:636.
413
- 414 11. Schmidt A, Kochanowski K, Vedelaar S, Ahrne E, Volkmer B, Callipo L, Knoops K,
415 Bauer M, Aebersold R, Heinemann M. 2016. The quantitative and condition-dependent
416 *Escherichia coli* proteome. *Nat Biotechnol* 34:104-10.
417
- 418 12. Klumpp S, Scott M, Pedersen S, Hwa T. 2013. Molecular crowding limits translation and
419 cell growth. *Proc Natl Acad Sci U S A* 110:16754-9.
420
- 421 13. Diaconu M, Kothe U, Schlunzen F, Fischer N, Harms JM, Tonevitsky AG, Stark H,
422 Rodnina MV, Wahl MC. 2005. Structural basis for the function of the ribosomal L7/12
423 stalk in factor binding and GTPase activation. *Cell* 121:991-1004.
424

- 425 14. Voorhees RM, Ramakrishnan V. 2013. Structural basis of the translational elongation
426 cycle. *Annu Rev Biochem* 82:203-36.
427
- 428 15. Savelsbergh A, Mohr D, Kothe U, Wintermeyer W, Rodnina MV. 2005. Control of
429 phosphate release from elongation factor G by ribosomal protein L7/12. *EMBO J*
430 24:4316-4323.
431
- 432 16. Savelsbergh A, Mohr D, Wilden B, Wintermeyer W, Rodnina MV. 2000. Stimulation of
433 the GTPase Activity of Translation Elongation Factor G by Ribosomal Protein L7/12. *J*
434 *Biol Chem* 275:890-894.
435
- 436 17. Dong H, Nilsson L, Kurland CG. 1996. Co-variation of tRNA Abundance and Codon
437 Usage in *Escherichia coli* at Different Growth Rates. *J Mol Biol* 260:649-663.
438
- 439 18. Uemura S, Aitken CE, Korlach J, Flusberg BA, Turner SW, Puglisi JD. 2010. Real-time
440 tRNA transit on single translating ribosomes at codon resolution. *Nature* 464:1012-7.
441
- 442 19. Chen C, Stevens B, Kaur J, Smilansky Z, Cooperman BS, Goldman YE. 2011. Allosteric
443 vs. spontaneous exit-site (E-site) tRNA dissociation early in protein synthesis. *Proc Natl*
444 *Acad Sci U S A* 108:16980-5.
445
- 446 20. Abdulkarim F, Ehrenberg M, Hughes D. 1996. Mutants of EF-Tu defective in binding
447 aminoacyl-tRNA. *FEBS Letters* 382:297-303.
448
- 449 21. Phillip Y, Schreiber G. 2013. Formation of protein complexes in crowded environments –
450 From in vitro to in vivo. *FEBS Letters* 587:1046-1052.
451
- 452 22. Dill K, Bromberg S. 2010. *Molecular Driving Forces: Statistical Thermodynamics in*
453 *Biology, Chemistry, Physics, and Nanoscience*. Garland Science.
454
- 455 23. Reeh S, Pedersen S. 1978. Regulation of *Escherichia coli* elongation factor synthesis *in*
456 *vivo*. *Gene Expression (11th FEBS Meeting Copenhagen 1977)*, eds Clark BFC, Klenow
457 H, Zeuthen J (Pergamon, Oxford),:89–98.
458